Materials Science Research International, Vol.2, No.1, pp.1-12 (1996)

Review paper

CHAOTIC ATOM MOTION EXCITED BY FRACTURE

Wei YANG and Honglai TAN

Department of Engineering Mechanics, Tsinghua University, Beijing 100084, P. R. China

Abstract: Many experimental phenomena concerning microscopic fracture processes have an atomistic origin. The crack tip atom motion excited by fracture is highly nonlinear and chaotic, rendering the atomistic and chaotic characterizations as essential aspects of fracture processes. In this article, we outline a combined atomistic-continuum formulism for material fracture studies. The chaotic atom motion near a crack tip is explored by using a simplified atom-continuum model, so that an analytical characterization is possible. The phenomena examined under this methodology include catastrophic atomistic cleavage, fracto-emisson, chaos in dynamic cleavage and chaotic dislocation emissions.

Key words: *Combined atom-continuum calculation, Catastrophe, Chaos, Cleavage, Dislocation emission*

1 INTRODUCTION

Many experimental phenomena concerning microscopic fracture processes have an atomistic origin. Atom motion near a crack tip is highly nonlinear and frequently of chaotic nature. This nonlinear and chaotic motion manifests to various macroscopic complexities observed in experiments. In this article, we formulate a combined atomistic-continuum computation scheme. A simplified model of this scheme provides us the desired analytical tractability, and enables us to explore the chaotic atom motion near a crack tip. The phenomena under examination include catastrophic atomistic cleavage, fracto-emission, chaos in the dynamic cleavage processes and chaotic dislocation emissions.

Atomistic chaos in materials fracture is generated from two types of interactions; from the interaction of many atoms and from the chaotic interaction of a single atom pair at the crack tip. In many-atoms scale, chaos may occur during dislocations emissions or damages evolution processes. Tens to thousands atoms surrounded the crack tip are involved in this process. If the number of the interacted atoms is small, the processes may be studied by a quasi-analytical approach, as outlined in sections 5 and 6. If the number of the interacted atoms is large, detailed molecular dynamic simulations are needed. In the mono-interatomic process, a combined atomistic-continuum approach may be adopted so that the attention can be focused on the chaotic motion of the crack tip atom pair. The two aspects of atomistic chaos in material fracture require different atomistic-continuum approaches. To simulate many-atom effects, thousands of atoms should be contained in an atomistic-continuum assembly, and the investigations can only be numerical. To get the essential information of the chaotic atom motion, on the other hand, only a few atoms are needed and their interaction with the surrounding continuum would be treated analytically. Most of the subsequent analyses will be focused on the second approach.

Received November 21, 1995

2 DESCRIPTION OF ATOMIC BONDING

The intrinsic fracture toughness of a material can be studied from an atomistic approach by means of a universal expression for the binding potential energy versus atomic separation curves [1]. A complete description of materials can be furnished from a first principle computation such as the *ab initio* calculation. However, the number of the macroscopic properties which can be obtained from such level is small. To make the atomistic studies practical, a classical or semi-classical potential, from which interparticle forces can be derived, is necessary. EAM and the modified EAM advanced by Daw and Baskes [2-5] provide a feasible formalism by which multi-body inter-atomic potentials may be constructed for various metallic solids. Furthermore, it readily allows the construction of potentials for solids which contain defects, interfaces, surfaces, etc. In EAM the total energy stored in a crystal lattice, E_{total}, is expressed by

$$E_{\text{total}} = \sum_i E_i, \tag{1}$$

where

$$E_i = \frac{1}{2}\Phi_i(\mathbf{r}_i) + F(\rho_i). \tag{2}$$

The first term on the right hand side characterizes the conventional pair potential, with Φ_i representing the core-core pair repulsion between the i-th atom (located at $\mathbf{r}_i$) and the rest of the atoms in crystal lattice. The second term $F(\rho_i)$ is the energy to embed atom i in a background of electron density ρ_i, where ρ_i denotes the host electron density at atom i due to a superposition of electron densities contributed by all atoms in the aggregate. The many-body effects described by the embedding energy function $F(\rho_i)$ gives more accurate description than the pair potential.

The classical pair formulation for the interatomic potentials assumes that all particles in a crystal are bonded by the central interaction between any paired-particles. Though it is a simplification, as a first prin-

ciple approximation it can be used to describe the interaction between atoms. For the metallic or covalent bonding, the following 6-9 potential [6] can be used

$$\Phi(r) = \Phi_0 \left[-3(\frac{a_0}{r})^6 + 2(\frac{a_0}{r})^9 \right], \qquad (3)$$

where Φ_0 is the reference interaction energy and a_0 is the reference interatomic distance.

For ionic bonding, Born's Theory gives the following interatomic potential

$$\Phi(r) = \frac{A}{r^s} - \alpha_M \frac{e^2}{4\pi\epsilon_0 r}, \qquad (4)$$

where s denotes a dimensionless exponent of about 10, A an interatomic bonding constant, α_M the Madelung constant, e the unit electron charge, and ϵ_0 the dielectric constant. Various constants for the above two descriptions can be found in [7].

When the interatomic potential is known, the interatomic force can be given by

$$f(r) = -\frac{d}{dr}\Phi(r). \qquad (5)$$

3 COMBINED ATOMISTIC-CONTINUUM FORMALISM

Atomic calculations have been carried out to explore the atom motion at the crack tip [8-15]. The calculations are performed for a side-cracked disc configuration under a remote K field loading. Using the molecular dynamics, Monte Carlo method and atom exchange technique, Tan and Yang [11] simulated several atomistic phenomena. It is revealed [11] that the brittle-to-ductile transition of homogeneous materials is defined by a critical loading rate, and the nanoscopic profile near an interfacial crack tip is dictated by the near tip mode mixity. The brittle-to-ductile transition via dislocation nucleation is observed in the molecular dynamics simulation [12].

Mullins and Dokainish[16], Kohlhoff *et al.* [17], Yang *et al.* [18] ,and Tan and Yang [19] performed a combined atomistic-continuum simulation on interfacial fracture. The model consists of a nanoscopic core made by atomistic assembly and a surrounding elastic continuum with discrete dislocations. In [17-19] an overlapping belt is designed to transmit mechanics parameters, such as displacements, stresses, masses and momentum, between the atomistic and continuum regions. In the model of Kohlhoff *et al.*, the overlapping layer is further divided into two parts under the frame of the non-local elasticity theory formulated by Kröner[20,21]. The method allows an effective coupling of the two media governed by different stress types. However models developed in [16,17] can not allow the permeability of the geometric discontinuity. The overlapping layer developed in [18,19] provides a permeable interface to allow defects such as dislocations to move from the atom assembly to the surrounded continuum. Dislocations nucleate from the atomistic crack tip region and then move to the continuum layer where they glide according to the dislocation dynamics curve. The curve of dislocation velocity versus crack tip distance shows a smooth velocity variation from the atomistic region to the continuum region.

The atomistic-continuum transmission is defined through matrices $\mathbf{T}^u_{L\leftarrow A}$ and $\mathbf{T}^f_{A\leftarrow L}$. In an overlapping layer, the atomistic description by molecular dynamics and the continuum description by finite elements(FE) co-exist. The displacement of a FE-node in the overlapping layer is averaged from a collection of atoms surrounding it. On the other hand, the element nodal forces are distributed to the surrounding atoms. The matrix $\mathbf{T}^u_{L\leftarrow A}$ conveys the atomistic displacements (labeled as "A") to the continuum FE nodes (labeled as "L"); and $\mathbf{T}^f_{A\leftarrow L}$ defines the transmission of forces from the continuum FE nodes to the atom assembly. These matrices obey the following transverse relation

$$\mathbf{T}^f_{A\leftarrow L} = (\mathbf{T}^u_{L\leftarrow A})^{\mathrm{T}}. \qquad (6)$$

The transmission formulae for the displacement, velocity, and force can be expressed as

$$\begin{aligned} \mathbf{u}_L &= \mathbf{T}^u_{L\leftarrow A}\mathbf{u}_A, \\ \dot{\mathbf{u}}_L &= \mathbf{T}^u_{L\leftarrow A}\dot{\mathbf{u}}_A, \\ \mathbf{f}_A &= \mathbf{T}^f_{A\leftarrow L}\mathbf{f}_L, \end{aligned} \qquad (7)$$

respectively.

The coupled atomistic/continuum simulation in [18,19] is facilitated by a *mechanical atmosphere* formed within the atom-continuum overlapping layer. In each time step, the continuum deformation induces atomic movements through the nodal forces generated on the overlapping belt. These nodal forces are converted to the forces acting on the overlapping atoms by matrix $\mathbf{T}^f_{A\leftarrow L}$. Under these applied atomic forces, the atoms assembly governed by the inter-atomic potential will update their positions. The new atomic configurations generate increments in displacements and momenta, which in turn modify the nodal displacements in the overlapping belt. The atomistic continuum interaction is evaluated iteratively. The atom oscillation at the crack tip is more frequent than that of the FE-node far from the crack tip. The simulation condenses most finite element degrees of freedoms to the matrices describing the mechanical atmosphere surrounding the atom assembly, leading to the reduction of the computation time.

The system potential is a functional of $\mathbf{u}_C(t)$, $\mathbf{u}_L(t)$ and $\mathbf{u}_A(t)$. Here the subscripts "C", "L"and "A"denote the freedoms belonging to the continuum, overlapping layer and atoms respectively. The potential of the whole system can be expressed as

$$\begin{aligned} &\Pi\left[\mathbf{u}_C(t), \mathbf{u}_L(t), \mathbf{u}_A(t)\right] \\ &= \tfrac{1}{2}\begin{pmatrix} \mathbf{u}_C^{\mathrm{T}} & \mathbf{u}_L^{\mathrm{T}} \end{pmatrix} \begin{pmatrix} \mathbf{K}_{CC} & \mathbf{K}_{CL} \\ \mathbf{K}_{LC} & \mathbf{K}_{LL} \end{pmatrix} \begin{pmatrix} \mathbf{u}_C \\ \mathbf{u}_L \end{pmatrix} \\ &- \begin{pmatrix} \mathbf{u}_C^{\mathrm{T}} & \mathbf{u}_L^{\mathrm{T}} \end{pmatrix} \begin{pmatrix} \mathbf{f}_C \\ \mathbf{f}_L \end{pmatrix} + \sum_{i\in A} E_i\left(\mathbf{u}_A\right). \end{aligned} \qquad (8)$$

The last term represents the energy in the atomistic assembly, with E_i given in Eq. (2). In the above expression, $\mathbf{K}_{CC}, \mathbf{K}_{CL}, \mathbf{K}_{LC}$ and $\mathbf{K}_{LL}$ are standard finite element stiffness matrices. (See Tan and Yang [19].)

In the overlapping belt, the continuum description and the atomistic description represent the same piece of material. In this sense, the above expression represents the potential of the whole system plus the potential in the overlapping belt. The double counting of potential energy in the overlapping belt, however, will not invalidate the field equations derived in the sequel. Since the field equations will take a local form, and will be homogeneous with the double counting factor, except along the boundary of the overlapping belt. Same situations will be encountered for the calculations of kinetic energy and the system Hamiltonian. We will skip the discussions on the double counting in the sequel for brevity.

The kinetic energy of the system is

$$\begin{aligned}&\mathrm{T}\left[\mathbf{u}_C(t), \mathbf{u}_L(t), \mathbf{u}_A(t)\right]\\&= \tfrac{1}{2}\begin{pmatrix}\dot{\mathbf{u}}_C^{\mathrm{T}} & \dot{\mathbf{u}}_L^{\mathrm{T}}\end{pmatrix}\begin{pmatrix}\mathbf{M}_{CC} & \mathbf{M}_{CL}\\ \mathbf{M}_{LC} & \mathbf{M}_{LL}\end{pmatrix}\begin{pmatrix}\dot{\mathbf{u}}_C\\ \dot{\mathbf{u}}_L\end{pmatrix}\\&+\tfrac{1}{2}\dot{\mathbf{u}}_A^{\mathrm{T}}\mathbf{M}_A\dot{\mathbf{u}}_A.\end{aligned} \tag{9}$$

where $\mathbf{M}_{CC}, \mathbf{M}_{CL}, \mathbf{M}_{LC}$ and $\mathbf{M}_{LL}$ are standard finite element mass matrices, and $\mathbf{M}_A$ is the mass matrix of the atom aggregate. The latter can be expressed as

$$\mathbf{M}_A = \begin{pmatrix} m_1 & & \\ & \ddots & \\ & & m_n \end{pmatrix}_{n\times n}, \tag{10}$$

where m_i $(i = 1, \cdots, n)$ is the mass of the atom i, and n is the total number of atoms.

The system Hamiltonian is given by

$$\begin{aligned}&H\left[\mathbf{u}_C(t), \mathbf{u}_L(t), \mathbf{u}_A(t)\right]\\&= \int_{t_1}^{t_2}\{\mathrm{T}\left[\mathbf{u}_C(t), \mathbf{u}_L(t), \mathbf{u}_A(t)\right]\\&-\Pi\left[\mathbf{u}_C(t), \mathbf{u}_L(t), \mathbf{u}_A(t)\right]\}dt.\end{aligned} \tag{11}$$

According to the Hamilton's principle, the Hamiltonian of the displacement fields should be stationary under actual motions $\mathbf{u}_C(t), \mathbf{u}_L(t)$ and $\mathbf{u}_A(t)$

$$\delta H\left[\mathbf{u}_C(t), \mathbf{u}_L(t), \mathbf{u}_A(t)\right] = 0. \tag{12}$$

In Eq. (12), all virtual displacements satisfying (i) boundary conditions, (ii) initial and ending conditions at $t = t_1$ and $t = t_2$ and (iii) the atomistic-continuum correspondence

$$\begin{aligned}\mathbf{u}_L(t) &= \mathbf{T}^u_{L\leftarrow A}\mathbf{u}_A(t),\\ \dot{\mathbf{u}}_L(t) &= \mathbf{T}^u_{L\leftarrow A}\dot{\mathbf{u}}_A(t)\end{aligned} \tag{13}$$

should be searched.

To introduce the constraints (13) into the Hamiltonian, we adopt the standard procedure of Lagrangian multipliers. The modified functional is

$$\begin{aligned}&H^*\left[\mathbf{u}_C(t), \mathbf{u}_L(t), \mathbf{u}_A(t), \boldsymbol{\lambda}_L(t), \boldsymbol{\mu}_L(t)\right]\\&= \int_{t_1}^{t_2}\{\mathrm{T}\left[\mathbf{u}_C(t), \mathbf{u}_L(t), \mathbf{u}_A(t)\right]\\&-\Pi\left[\mathbf{u}_C(t), \mathbf{u}_L(t), \mathbf{u}_A(t)\right]\\&+\left(\mathbf{u}_L(t) - \mathbf{T}^u_{L\leftarrow A}\mathbf{u}_A(t)\right)^{\mathrm{T}}\boldsymbol{\lambda}_L(t)\\&+\left(\dot{\mathbf{u}}_L(t) - \mathbf{T}^u_{L\leftarrow A}\dot{\mathbf{u}}_A(t)\right)^{\mathrm{T}}\boldsymbol{\mu}_L(t)\}dt.\end{aligned} \tag{14}$$

By the variational principle, among all the available displacements satisfying the above constraints (i) and (ii), the first variation of the modified functional would vanish by the actual displacements

$$\delta H^*\left[\mathbf{u}_C(t), \mathbf{u}_L(t), \mathbf{u}_A(t), \boldsymbol{\lambda}_L(t), \boldsymbol{\mu}_L(t)\right] = 0. \tag{15}$$

The above variational equation enables us to derive displacement field equations. By Eqs. (8) and (9), one can eliminate the Lagrange multipliers $\boldsymbol{\lambda}_L$ and $\boldsymbol{\mu}_L$. Through straightforward algebras, the governing equation of the atom aggregate is expressed by

$$\left(\mathbf{M}_A + \hat{\mathbf{M}}_A\right)\ddot{\mathbf{u}}_A = \mathbf{f}(\mathbf{u}_A) + \hat{\mathbf{F}}_A + \hat{\mathbf{P}}_A - \hat{\mathbf{K}}_{AA}\mathbf{u}_A. \tag{16}$$

The mechanical atmosphere surrounding the atom aggregate is prescribed by the following parameters

$$\hat{\mathbf{F}}_A = \mathbf{T}^f_{A\leftarrow L}\left(\mathbf{f}_L - \mathbf{K}_{LC}\mathbf{K}_{CC}^{-1}\mathbf{f}_C\right), \tag{17}$$

$$\hat{\mathbf{K}}_{AA} = \mathbf{T}^f_{A\leftarrow L}\left(\mathbf{K}_{LL} - \mathbf{K}_{LC}\mathbf{K}_{CC}^{-1}\mathbf{K}_{LC}\right)\mathbf{T}^u_{L\leftarrow A}, \tag{18}$$

$$\hat{\mathbf{P}}_A = \mathbf{T}^f_{A\leftarrow L}\left(\mathbf{K}_{LC}\mathbf{K}_{CC}^{-1}\mathbf{M}_{CC} - \mathbf{M}_{LC}\right)\ddot{\mathbf{u}}_C, \tag{19}$$

$$\hat{\mathbf{M}}_A = \mathbf{T}^f_{A\leftarrow L}\left(\mathbf{M}_{LL} - \mathbf{K}_{LC}\mathbf{K}_{CC}^{-1}\mathbf{M}_{CL}\right)\mathbf{T}^u_{L\leftarrow A}, \tag{20}$$

where $\hat{\mathbf{F}}_A$, $\hat{\mathbf{K}}_{AA}$ and $\hat{\mathbf{P}}_A$ are the forces, elastic constraints, and the D'Alembert inertia forces of the continuum acting on the atoms in the overlapping belt. The matrix $\hat{\mathbf{M}}_A$ denotes the additional masses adhered to the overlapping atoms.

Atomic motions in the area surrounding the crack tip are much faster than the nodal velocities in the continuum region. For an averaging quasi-static motion, one has

$$\begin{aligned}\ddot{\mathbf{u}}_C &= \mathbf{0},\\ \ddot{\mathbf{u}}_L &= \mathbf{0}.\end{aligned} \tag{21}$$

In this case one have the simplification

$$\begin{aligned}\hat{\mathbf{P}}_A &= \mathbf{0},\\ \hat{\mathbf{M}}_A\ddot{\mathbf{u}}_L &= \mathbf{0}.\end{aligned} \tag{22}$$

Under this algorithm, Yang *et al.* [18] and Tan and Yang [19] calculated the dislocation emission from an interfacial crack tip. Dislocations can be generated in the atomistic region by molecular dynamics calculations, and emitted from the crack tip as atomistic dislocations. They are switched to continuum dislocations in the overlapping zone, and travel to the continuum region outside. The simulation reveals that the nature of dislocation emission is greatly influenced by the zigzag interface structure.

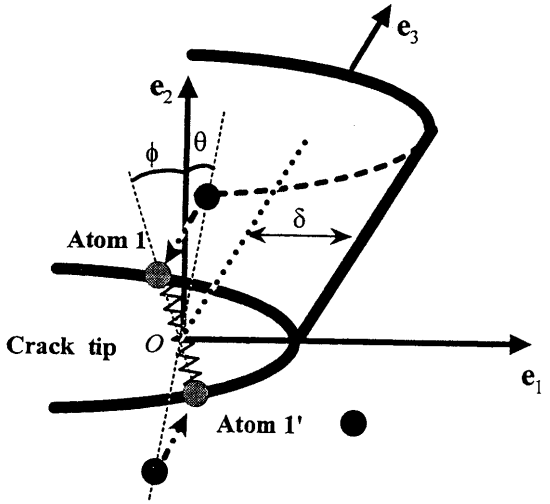

Fig. 1. Crack tip model for plane strain problem. Atoms in 3-dimensional configuration are projected to the plane perpendicular to direction. The solid circles refer to the 3-dimensional lattice atoms, the shaded ones refer to the projected atoms.

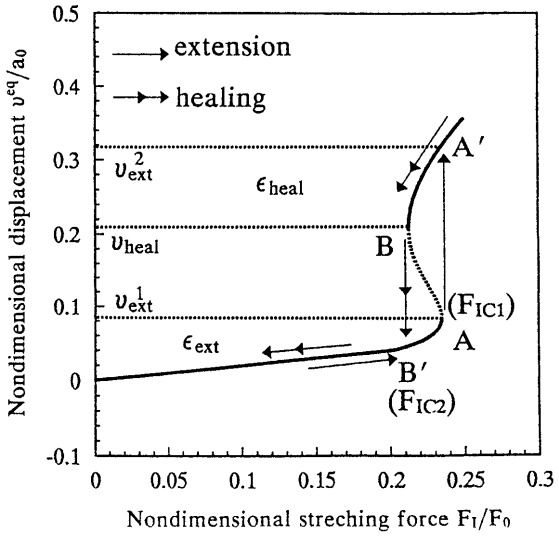

Fig. 2. Catastrophic jump of the equilibrium position of the crack tip atom during the cleavage process. The solid curves refer to stable states and the dashed curves to unstable states.

4 FRACTO-EMISSIONS DURING CATASTROPHE CLEAVAGE

4.1 Catastrophic Cleavage

Consider an ideal situation of averaging plane strain deformation. The three-dimensional atomic motions (solid particles) can be studied by their projections (shaded images) onto the plane perpendicular to $\mathbf{e}_3$ direction, as depicted in Fig. 1. As the simplest model of combined atomistic-continuum calculation, the atomistic region only consists of a string of two atoms (or an array of the similar atom strings in the thickness direction). The atom string locates at the crack tip and is embedded in the surrounding continuum. The three-dimensional atom string line orients at an angle θ with $\mathbf{e}_2$ axis in the figure. The angle θ reflects the actual three-dimensional lattice structure. When projecting it to a plane normal to $\mathbf{e}_3$, the projection forms an angle ϕ with $\mathbf{e}_2$ axis. For the cleavage case, the continuum stress field surrounding the crack tip is symmetric and is measured by a remote mode I stress intensity factor K_I. For the crack tip atoms, it was shown that the Newton's second law leads to [22,23]

$$m\ddot{v} = -\frac{d}{dv}U\left(v; F_I, E'\right), \tag{23}$$

where m is the mass of atom, v is the vertical displacement of the atom, $E' = E/\left(1-\nu^2\right)$, with the Young's modulus E and the Poisson's ratio ν. The cleavage potential $U\left(v; F_I, E'\right)$ has the following expression

$$U(v; F_I, E') = \frac{1}{2}\Phi\left(r(v)\right) - F_I v + \frac{1}{2}k_I\left(E'\right)v^2, \tag{24}$$

where $r(v)$ is the distance between the two atoms at the crack tip. The surrounding continuum exerts two effects on the movement of the atoms. One is the stretching effect due to the remote stress intensity factor, expressed as the work of the stretching force F_I against the vertical displacement v; and the other is the confining effect by the continuum against the atom vibration, where the effective stiffness of the cracked continuum is denoted by $k_I\left(E'\right)$. In the above expression, they are [22]

$$\begin{aligned} F_I &= 0.818K_I a_0^{3/2}, \\ k_I &= 0.513E'\delta, \end{aligned} \tag{25}$$

where δ denotes the distance between the interception of the atom string at the crack plane and the crack front, as shown in Fig. 1. The above two equations are simplified versions of Eqs. (17) and (18) respectively. In the present case, only two crack tip atoms are considered in the atom assembly. The $U(v; F_I, E')$ curves at different F_I values would predict a cleavage process featured by catastrophe, as will be discussed below.

Taking the special case of $a_0 = 4$Å , $m = 1.0 \times 10^{-25}$kg, $\Phi_0 = 2.22$eV, $E' = 84.2$GPa and a simple cubic lattice structure with the interatomic potential given by Eq. (3). Under a prescribed F_I, the equilibrium displacement $v^{eq}(F_I)$ curve for this representative case is shown in Fig. 2. That curve shows the fold catastrophe with the fold points at A and B, they give two critical values F_{IC1} and F_{IC2}. When $F_I < F_{IC2}$ or $F_I > F_{IC1}$, there is an one to one correspondence on the $v^{eq}(F_I)$ curve, and the solution is stable against perturbation. When $F_{IC2} < F_I < F_{IC1}$, three balanced positions exist, as shown in Fig. 2. The positions on the top and on the bottom are stable, while the one in the middle is unstable, and is depicted in dashed curves. The reference force in the figure is $F_0 = 0.818a_0^2E'$.

Figure 2 reveals a negative hysteresis loop during loading and unloading cycles. When the load F_I increases from a low value up to F_{IC1} , the crack tip atoms will catastrophically jump upward from state A to state A'. On the other hand, when the applied force reduces from a high value down to F_{IC2}, the crack tip atoms will catastrophically jump downward from state B to state B'. The unilateral jumping amplitude for one atom ranges from $0.15\sim0.25a_0$. The two catastrophic jumps of atom positions suddenly release potential energies during and after fracture, as observed by the experiments of Dickinson *et al.* [24]. From representative calculations in Fig. 2, the catastrophic jump of the system from state A to state A' (loading) gives an energy release of $\Delta E_1 = 0.18$eV, and that from state B to state B' (unloading) gives a smaller energy release of $\Delta E_2 = 0.10$eV.

To perform a static analysis on the atom response at the crack tip, Hsieh and Thomson [25] and Thomson *et al.* [26] developed the lattice Green's function (also called lattice statics) method. Using the crack tip lattice model, they studied the fracture behavior of brittle materials such as semiconductors and ceramic materials [27] and crack-dislocation effects in the fracture of crystalline materials [28]. The lattice Green's function approach gives the static response of the lattice under an applied force. In their model, linear atomic forces are assumed, except for those atoms in the verge of breaking. With this assumption they studied the static response of a single kink at the crack tip. The function of the external force versus the displacement at the origin is calculated and leads to the similar results as shown in Fig. 2. The model advanced by Tan and Yang [22,23] provides an analytical description of the crack tip atom motion, combining the atomic motion with the surrounding continuum.

In addition to the catastrophic jumps, a periodic irreversible energy barrier is encountered during the cleavage process. This energy barrier is called the Lattice Trapping Barrier (LTB). As shown in Fig. 2, the top side crack tip atom jumps from $v^1_{\rm ext}$ to $v^2_{\rm ext}$ under the applied force F_{IC1}. Under the force F_{IC2}, the atom will jump from the displacement of $v_{\rm heal}$ back to the bottom curve. The LTB for crack extension can be expressed as

$$\mathcal{E}_{\rm ext} = \int_0^{v^1_{\rm ext}} F(v)\mathrm{d}v, \tag{26}$$

and LTB for crack healing as

$$\mathcal{E}_{\rm heal} = -\int_{v^2_{\rm ext}}^{v_{\rm heal}} F(v)\mathrm{d}v. \tag{27}$$

From Fig. 2, we observe that the when there is a catastrophic jump of the loading curve, $F(v)$ in the above two integrations has different paths. We have

$$\mathcal{E}_{\rm heal} > \mathcal{E}_{\rm ext}. \tag{28}$$

Sinclair [29] studied silicon and found a two-dimensional lattice-trapping barrier for forward crack motion of about $0.25e_0$. Markworth and Hirth [30]

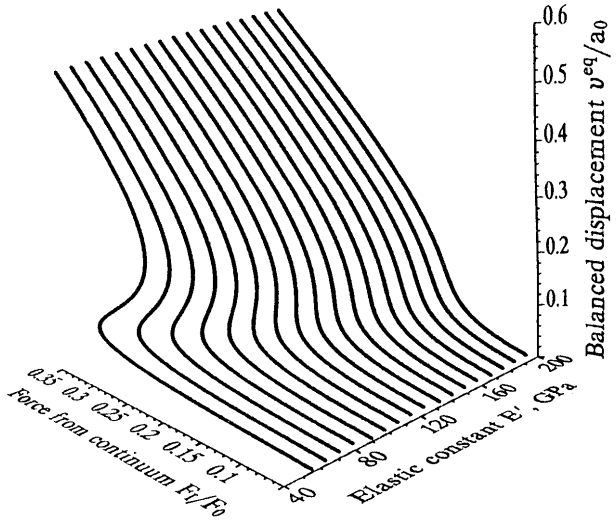

Fig. 3. Three-dimensional portrait of the surface $v^{\rm eq}(E', F)$ shows a cusp catastrophe. Each line in the surface corresponds to a specific material characterized by the elastic constant E' .

devised a model consists a system of four point mass atoms, arranged along a straight line by identical Morse-function "springs". The model show a marked asymmetry in the magnitudes of the barriers.

4.2 Fracto-Emissions

Experiments on fracture processes show the emission of particles, including photons, electrons, ions and neutral species, during and after the fracture of materials [31-35]. These phenomena are collectively termed fracto-emissions because the material fracture is a prerequisite for their appearance. The transport of fracto-emissions has proved to be a useful probe on the local environment in materials if that transport is dictated by the local geometry. Experiment by Langford et al. [36] took the photon emission as a probe of chaotic processes accompanying fracture. The spectrum of emitted particles are served as measurements for the fractal crack path and the chaotic emission process.

The fracto-emission phenomenon may be explained using the present catastrophic cleavage theory. The crack tip atomic potential drops when the crack advances. The released potential energy converts into the kinetic energy of the crack tip atoms. Two channels exist to absorb or to diffuse this kinetic energy. One is through the excitation of fracto-emissions, and the other is through the wave propagation. Fracto-emissions will be excited when the energy impulse is sufficiently high and cannot be effectively carried away by wave propagation. The probability of the fracto-emission may assume an Arrhenius form

$$\text{prob} = \min\left[\exp\left((\Delta E - \widehat{E})/(k_B T)\right), 1\right], \tag{29}$$

Table 1. Fracto-emission analysis on representative materials.

(a) Ionic crystals of NaCl structure, cleavage system (001)[100]

Crystal	a_0, Å	A, eV $\cdot$ (Å)^s	s	E', GPa	E'_C, GPa	ΔE_1, eV	ΔE_2 , eV
LiF	2.01	1.63×10^2	6.20	108	314	3.18	1.05
NaCl	2.82	6.98×10^3	8.38	43.4	109	2.30	0.926

(b) Metallic crystal of f.c.c. structure, cleavage system (001)[110]

Crystal	a_0, Å	Φ_0, eV	E', GPa	E'_C, GPa	Fracto-emissions
Cu	2.55	0.391	147	102	No
Al	2.86	0.359	79.8	66.6	No

(c) Metallic crystal of b.c.c. structure, cleavage system (001)[100]

Crystal	a_0, Å	Φ_0,eV	E', GPa	E'_C, GPa	Fracto-emissions
Fe	2.48	0.780	231	155	No
W	2.74	1.57	446	230	No

(d) Covalent crystal of diamond cubic structure, cleavage system (111) [0$\bar{1}$1]

Crystal	a_0, Å)	Φ_0, eV	E', GPa	E'_C, GPa	ΔE_1, eV	ΔE_2, eV
C	1.54	3.59	1.09×10^3	2.46×10^3	0.644	0.660
Si	2.35	2.16	154	416	0.764	0.488
Ge	2.45	1.96	123	334	0.688	0.445

where k_B is the Boltzmann's constant, T the absolute temperature, ΔE the energy released by catastrophe and $\widehat{E}$ the energy barrier (0.2eV to 2eV) to cause a particle emission. Take the example of the fracto-emission of NaCl monomers. Experiments [37] indicate that the emission of an NaCl monomer from a defect-free flat surface requires 2.2eV. The energy required for fracture related emission should be considerably lower than that. The sublimation energy on a cracked surface of NaCl is about 0.25eV [37].The available time for fracto-emission, $t_{\rm frac}$, can be estimated from the crack propagation velocity. The crack velocity can be estimated from the light transmission measurements [38]. The time interval $t_{\rm frac}$ for fracto-emissions ranges from 100ps (slow cleavage) to 0.2-1ps (fast cleavage). Fracto-emissions are easily induced during fast cleavage, since the excitation energy is supplied continuously at high intensity. We now investigate the slow cleavage case where $t_{\rm frac}$ is about 100ps. This time interval is much larger than the dynamic characteristic time $t_{\rm wave}$, the time interval for the stress wave to travel away. Typical data give the order of $t_{\rm wave}$ in the range of 0.1-0.2ps. For the slow cleavage case, we have $t_{\rm frac} \gg t_{\rm wave}$, and a quasi-static approximation can be applied to the governing equation (23). The time duration for this catastrophic energy release can be estimated from

$$t_{\rm jump} = v_{\rm jump}/c_{\rm jump}, \tag{30}$$

wher $v_{\rm jump} = v^2_{\rm ext} - v^1_{\rm ext}$ is the jump value of the vertical displacement at catastrophe. The jumping velocity of the bond-broken atom, $c_{\rm jump}$, can be estimated as follows. The potential energy jump ΔE of the atom pair is transformed into the kinetic energy $mc^2_{\rm jump}$ of two symmetric atoms at the crack tip. Thus $c_{\rm jump}$ equals to

$$c_{\rm jump} = \sqrt{\frac{\Delta E}{m}}. \tag{31}$$

Combining Eqs. (30) and (31), one finds the time interval in the opening jump for the atom pair is about 0.18ps, if the unilateral vertical jump is $v_{\rm jump} = 0.25a_0$. This jump time is relatively short, so that the energy impulse released during the catastrophe cannot be taken away by wave dispersion and is supplied to cause fracto-emissions.

Under a prescribed F_I value, the equilibrium solution $v^{\rm eq}$ depends critically on E'. Figure 3 shows the surface $v^{\rm eq}(E', F_I)$. This graph has the structure of a cusp catastrophe. The curve on surface where the upper and lower sheets fold over into the middle sheet is called the fold-curve. The projection of this curve onto the horizontal controlling plane forms the bifurcation set, which defines the bounds for energy releases. In most cases, the intensities of fracto-emissions reach their peak *during* the fracture event and decay afterward. However, recent measurements also showed rapid, intense bursts of atomic and molecular emissions that arise *after* the fracture. The bifurcation set in Fig. 3 explains the catastrophic energy releases, and consequently emission bursts, during the loading and unloading phases of cleavage.

Although the fold curve is a smooth one, the bifurcation set has a sharp point. The cusp point provides a critical value for the material parameter E', denoted as E'_C. Accordingly, a criterion for the material to have a catastrophic jump can be phrased by the comparison between E' and E'_C

$$E' < E'_C, \tag{32}$$

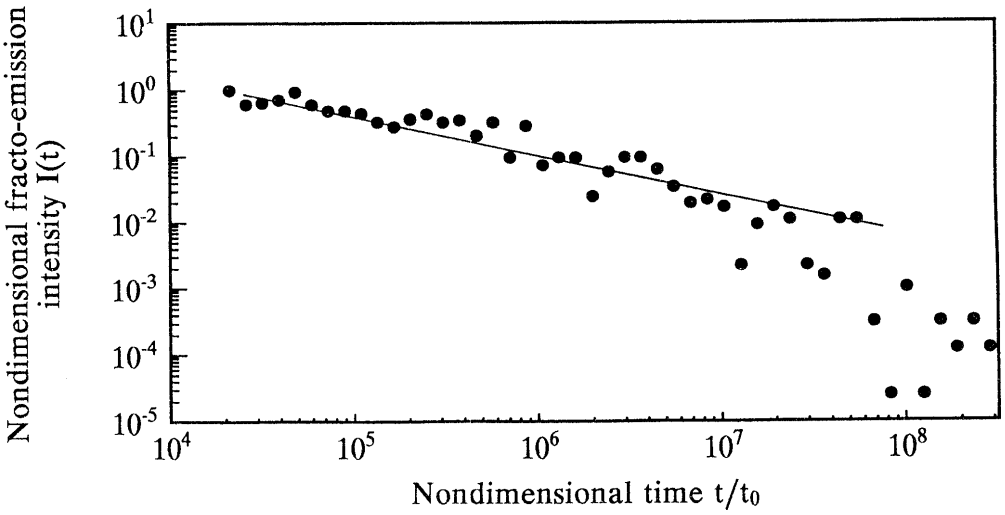

Fig. 4. Log-log curve of the fracto-emission intensity versus time for the after-peak decay period.

where

$$E'_C = -\frac{0.975}{\delta} \max_{0<v<\infty} \left[\frac{d^2\Phi}{dr^2} \left(\frac{dr}{dv} \right)^2 + \frac{d\Phi}{dr} \frac{d^2r}{dv^2} \right] \quad (33)$$

Table 1 lists relevant data for several representative materials based on the present theory for slow cracking. The parameter values for the interatomic potentials a_0, Φ_0, E', A, and s are taken from the experiment data, [7,39-41]. ΔE_{ext} and ΔE_{heal} refer to the energies released in the extending and healing processes, respectively. Some materials listed in the table are ductile under normal conditions and the fracture process is mainly controlled by dislocation emissions. The results in Table 1 indicate that we can hardly observe fracto-emission in metallic crystals. The fracto-emission for ionic and covalent crystals can be easily observed. The catastrophic energy release under these materials varies from 0.45eV to 1.1eV, sufficient to induce fracto-emission.

4.3 Effect of a Zigzag Channel

Tsai and Mecholsky[42] studied the fractal fracture of single crystal silicon. The self-similar nature of fracture offers a way that the relationship between bond breaking at the crack tip and the fracture surface morphology can be found. The nature of this phenomena may be related to the self-similar pre-fracture zone growth in the vicinity of the propagated crack tip. Experimental observations show the relation between the fracture toughness and fractal crack [43-45]. Scanning tunneling microscope observations of LiF fracture surfaces indicate that they can be very rough on nanoscopic scale [46]. A simple quantitative description for an irregular surface was to model it as a zigzag surface, as shown in the schematic profiles in [46].

Using the zigzag profile model, Tan and Yang [23] presented a numerical simulation of the fracto-emission process channeled by the cracked surfaces. The result suggests that the long-lasting tail observed in the photon emissions is caused by the zigzag character of crack surfaces. Figure 4 shows the simulated dimensionless fracto-emission intensity $I(t)$ under the zigzag fracture surface model, where $I(t)$ is the particle beam intensity normalized by its maximum value. The results are presented by a log-log plot of the after-peak fracto-emission intensity versus time. The relation between $\log(I(t))$ and $\log(t/t_0)$ is roughly linear, which suggests

$$I(t) \propto \left(\frac{t_0}{t} \right)^{\beta}, \quad (34)$$

in agreement to the experimental observations [24]. In the above equation, t_0 is the time for a particle to fly over the crack with ideally flat surfaces. From the slope of the log-log curve, we estimate that $\beta = 0.63$.

5 CHAOTIC CLEAVAGE PROCESSES

It is well known that certain systems exhibit chaotic behavior. Nip *et al.* [47] constructed equations of atomic motion in a two-dimensional crystal lattice and studied the chaotic phenomena. Numerical analysis indicates that the system integrability depends on its energy level. The breaking of the crack tip atomic bond is a dynamic and highly nonlinear process. Markworth and Hirth [30] proposed a simple atomic model for a crack tip, consisting of a string of four atoms. Markworth later [48] described certain catastrophic behavior this crack tip model may exhibit. Dynamic calculations are carried out by pinning the two end atoms while allowing the two inner atoms to move freely. Upon large departures from the state of minimum potential energy, the inner atom motion was shown to be chaotic [49,50].

Mohan *et. al.* [51] extended the above model to study the effects of dissipation and excitation on the chaotic dynamics in a cleavage process. Damping is introduced by dissipative mechanisms occurring at the crack tip. Chaotic motion is found under large excitations and small damping constants. The models by Markworth *et. al.* [50] and by Mohan *et. al.*

[51], however, only consists of one dimensional array of four atoms, connected by nearest-neighbor inter-atomic bonds. Linking the atom-string model to a continuum mechanical field characterized by K_I, Tan and Yang [22] present a model to elucidate that how the surrounding continuum mechanics field controls the near crack tip atom motion. Consider the four-atom string model for a crack tip. The nonlineality in the inter-atomic force law of these atoms will be shown to generate chaos during a cleavage process. By the symmetry of the problem, only the two atoms (labelled by subscripts 1 and 2) above the crack extension line need to considered. Let $\xi_1 = v_1$, $\xi_2 = m\dot{v}_1$, $\xi_3 = v_2$ and $\xi_4 = m\dot{v}_2$, one can formulate the atom motions by a system of first order differential equations

$$\begin{aligned} \dot{\xi}_1 &= \xi_2/m, \\ \dot{\xi}_2 &= -f(a_0 + \xi_3 - \xi_1) + f(a_0 + 2\xi_1), \\ \dot{\xi}_3 &= \xi_4/m, \\ \dot{\xi}_4 &= F - k\xi_3 + f(a_0 + \xi_3 - \xi_1), \end{aligned} \tag{35}$$

where the interatomic force f is given by Eq. (5). Homogeneous initial condition is assigned in the subsequent numerical simulation.

The above dynamic system may excite chaotic behavior. Lyapunov exponents measure the expansion or contraction along different directions in the phase space and are among the most useful quantities in characterizing chaotic systems. Given a continuous dynamic system in an n-dimensional phase space, an infinitesimal n-sphere will become an n-ellipsoid in the long-term evolution. Denoting the length of the sphere along the i-th dimension by $p_i(t)$, one can define the Lyapunov exponents as

$$\lambda_i = \lim_{t\to\infty} \frac{1}{t} \log_2 \frac{p_i(t)}{p(0)}, i = 1, 2, \cdots, n. \tag{36}$$

Their algebraic values are ordered from large to small as $\lambda_1 \geq \lambda_2 \geq \ldots \geq \lambda_n$. Wolf *et. al.* [52] provided an algorithm to search all Lyapunov exponents. A positive Lyapunov exponent is the conclusive evidence for chaos, and reflects the time scale over which the evolution of a dynamic system becomes unpredictable.

In Fig. 5, the largest Lyapunov exponent of the dynamic system (35) is calculated for the load parameter $\alpha = K_I/K_0$ varying from 0 to 0.5, where $K_0 = E'\sqrt{a_0}$. The largest Lyapunov exponent can be evaluated directly from the exponential growth on the separation of initially neighboring trajectories. The whole simulation consists of one million Lyapunov restarting steps. The Lyapunov exponent analysis on the equation system governed by Eq. (35) is drawn in Fig. 5. As the load parameter α increases, the crack tip atoms exhibit four types of dynamic responses. For an α value in regime I, atoms vibrate individually near the balanced positions. In regime II, nonlinear effect dominates and atoms couple together to approach a state of bond breaking. The maximum Lyapunov exponent rises suddenly at an α value (about 0.1) considerably smaller than the one of the static fracture toughness

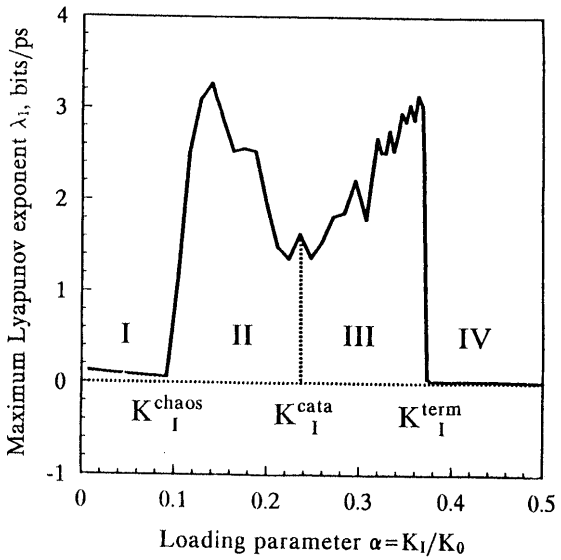

Fig. 5. The maximum Lyapunov exponent λ_1 versus the load parameter α.

(α =0.235). Consequently, the crack tip chaotic atom motion is a precursor of cleavage. In regime III, bond breaks from the static point of view, but the weakened interaction still holds the atom pair together. At even higher load in section IV, the linearity of the system is recovered and the nonlinear bonding between the atom pair is completely lost. The two broken atom string segments are hooked to the upper and lower crack faces and vibrate with the continuum. The crack moves to the next atom pair.

The result in Fig. 5 suggests that the dynamic fracture process is a more complex procedure than the static one. K_I^{cata} is the value of K_I at which the crack tip atom jumps catastrophically to extend the crack. From the figure we can get two additional parameters for dynamic cleavage, namely the K_I^{chaos} value at the transition from section I to section II and the K_I^{term} value at the transition from section III to IV. K_I^{chaos} refers to the burst of chaos in a dynamic process. When $K_I^{chaos} > K_I$, the crack is absolutely stable and remains stationary. When $K_I^{chaos} < K_I < K_I^{cata}$, chaotic atom motion occurs prior to complete cleavage separation. Small disturbances (such as the loading rate fluctuations and temperature induced fluctuations on the phase trajectories through Brownian motion) may have significant influences on the dynamic motion of crack tip atoms, and the spatial region for atoms under chaotic motion may spread. This corresponds to a diffusive fracture process. K_I^{term} refers to the termination of chaos in the dynamic process of the crack tip atoms. When the stress intensity factor exceeds this value, disastrous fracture occurs with the crack moving ahead without stop.

Besides its meaning in mathematics, chaos has certain meanings in a cleavage process. As a precursor to cleavage fracture, chaotic motion characterizes a period of time on the cleavage process when the inter-atomic bond disintegrates under certain cohesion. The critical values for the chaos to occur and to recede link

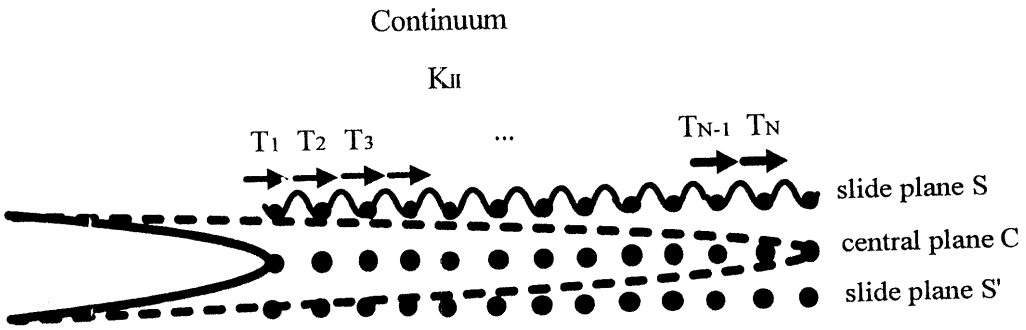

Fig. 6. Dislocation emission band model.

to various fracture parameters, and their meanings to a dynamic cleavage process are yet to be explored.

6 CHAOTIC DISLOCATION EMISSION

Rice [53] discussed the equilibrium (or static) process of dislocation emission from a crack tip based on the Peierls concept. A slip plane with periodic shear stress and sliding displacement relation is embedded in an elastic continuum to incorporate the continuum elasticity with an atomistic description of the dislocation core. Rice's static analysis introduces a new solid state parameter: the unstable stacking energy. Recently, Sun *et al.* [54] extended this model to the case of tension-shear coupling in the dislocation nucleation from a crack tip.

The above models for dislocation emission at the crack tip does not incorporate the dynamic atom motion. It is the pattern of this dynamic motion near the crack tip that dictates the failure modes of solids, and provides more accurate description for their brittle versus ductile behavior. The dislocation nucleation at the crack tip was studied by Doyama [55] by means of molecular dynamics method with an analytical model. For the complete procedure of atomistic dynamic emission of dislocations, a simple model is formulated as follows, Tan and Yang [56].

In the subsequent analyses, the crack is viewed as a semi-infinite slit in an otherwise unbounded solid, loaded at the infinity through a crack tip singularity field. Consider the anti-symmetric mode II loading by the stress intensity factor K_{II}. Ahead of the semi-infinite crack in the continuum, a number of atom columns (connecting each other by inter-atomic bonds) is positioned and embedded in the cracked continuum. We term this strip a dislocation emission band. One possible configuration of the dislocation emission band is shown in Fig. 6. N columns of atoms ahead of the crack tip are included. We attempt to analyze the dynamic motion of a dislocation core along this dislocation emission band.

Denote the horizontal displacement of atom i in the sliding plane S as u_i. The shear stress acting on the atom in the balanced configuration is the summation of horizontal components of forces exerted from all atoms in the central plane

$$\tau_i(u_i) = \frac{1}{a_0^2} \sum_{j=c_1}^{c_N} f\left(|\mathbf{r}_{ij}|\right) \frac{\mathbf{r}_{ij}\cdot\mathbf{e}_1}{|\mathbf{r}_{ij}|}, \tag{37}$$

where $\mathbf{r}_{ij} = \mathbf{r}_i - \mathbf{r}_j$.

The Peierls concept gives rise to an alternative way to obtain the shear stress τ along the slip plane. The function $\tau_i(u_i)$ would assume the same form for any atom i if the presence of the crack has negligible influence on the slide potential. Accordingly, $\tau_i(u_i)$ can be approximated as $\tau(u_i)$, a periodic function of the atomic displacement u_i with the period a_0. The simplest form of $\tau(u_i)$ is the Frenkel sinusoidal function

$$\tau(u_i) = \frac{\mu_{\text{slip}}}{2\pi} \sin(2\pi u_i/a_0). \tag{38}$$

When u_i is small, $\tau(u_i)$ degenerates to $-\mu_{\text{slip}} u_i/a_0$. The modulus, μ_{slip} , refers to the shear resistance of central atom plane C against the sliding atom plane S. Matching the amplitudes of the periodic functions (37) and (38), we get $\mu_{\text{slip}} = 3.04\Phi_0/a_0^3$.

Now we determine the forces F_i and constraints k_i exerted from the continuum to the i-th sliding atom, under the framework of linear fracture mechanics. The horizontal displacement can be expressed by the following superposition

$$u_i(t) = u_i^K + u_i^T(t), \tag{39}$$

where u_i^K is the background displacement caused by the stress intensity factor K_{II}, and $u_i^T(t)$ is the crack tip atom vibration. u_i^K is given by the well-known K-field,

$$u_i^K = \frac{2K_{II}}{E'} \sqrt{\frac{2(N+1-i)a_0}{\pi}}. \tag{40}$$

The term $u_i^T(t)$ is induced by a pair of transversal concentrating forces $T_i(t)a_0^2$ applied on the upper and lower slit faces of the cracked continuum. A remarkable result by Freund [57] indicated (see also Tan and Yang [22,56]) that the relation between $T_i(t)$ and $u_i^T(t)$ can be approximately expressed by their quasi-static relation at a time scale much larger than 0.2ps.

Namely

$$T_i(t) = -\frac{1}{\beta(N+1-i)}\frac{\pi E'}{a_0}u_i^T(t), \tag{41}$$

where

$$\begin{aligned}\beta(n) &= 2\sqrt{4n^2+2n} \\ &+\ln\left(2\sqrt{4n^2+2n}+4n+1\right) \\ &-2\sqrt{4n^2-2n} \\ &+\ln\left(2\sqrt{4n^2-2n}+4n-1\right).\end{aligned} \tag{42}$$

Combining the above three expressions, one gets the force acting on atom i as

$$F_i = 2\frac{\sqrt{2(N+1-i)}}{\beta(N+1-i)}K_{II}\sqrt{\pi a_0}a_0 \tag{43}$$

and the continuum confinement to atom i is

$$k_i = \frac{1}{\beta(N+1-i)}\pi E' a_0. \tag{44}$$

For a dislocation emission band ahead of the crack tip, the system Hamiltonian is

$$\begin{aligned}H = &\sum_{i=1}^{N}\left(\tfrac{1}{2}m\dot{u}_i^2 - F_i u_i + a_0\tfrac{\mu_{\rm slip}+k_i a_0}{2\pi^2}\sin^2\tfrac{\pi u_i}{a_0}\right) \\ &+\sum_{i=2}^{N}\Phi(u_i-u_{i-1}).\end{aligned} \tag{45}$$

The summation in Eq. (45) is carried over all atom columns. Denote $\xi_{2i-1}=u_i$, $\xi_{2i}=m\dot{u}_i$, one can write a system of differential equations by

$$\begin{aligned}&\dot{\xi}_1 = \xi_2/m, \\ &\dot{\xi}_2 = -\tfrac{a_0}{2\pi}\left(k_1+\mu_{\rm slip}a_0\right)\sin\left(2\pi\tfrac{\xi_1}{a_0}\right) \\ &\qquad -f(r_{12})+F_1, \\ &\dot{\xi}_{2i-1} = \xi_{2i}/m,\ 2\le i\le N, \\ &\dot{\xi}_{2i} = -\tfrac{a_0}{2\pi}\left(k_1+\mu_{\rm slip}a_0\right)\sin\left(2\pi\tfrac{\xi_{2i-1}}{a_0}\right) \\ &\qquad -f(r_{i,i+1})+f(r_{i-1,i})+F_i,\ 2\le i\le N.\end{aligned} \tag{46}$$

At the end of the dislocation emission band, equilibrium conditions are enforced

$$\begin{aligned}&u_{N+1}=0, \\ &f(r_{N,N+1})=0.\end{aligned} \tag{47}$$

Namely atoms along the tail of a dislocation emission band are held in the undeformed lattice.

We investigate the critical value for dislocation emission $K_{II}^{\rm emit}$ when the number of atom columns, N, in the dislocation emission band varies from 1 to several tens. $K_{II}^{\rm emit}$ can be evaluated from a static analysis. Taking the left hand side of Eq. (46) to be zero, we get N equations, with $N+1$ unknowns ξ_1 , ξ_3 ,..., ξ_{2N-1} , and K_{II}. Selecting a sequence of ξ_1 values from 0 to a_0 , one can solve the nonlinear equations described above and predict the values of K_{II} at specific ξ_1 values. The peak value of the K_{II} versus ξ_1 curve gives the value of $K_{II}^{\rm emit}$. If one proceeds in this way, each N will lead to a corresponding value of $K_{II}^{\rm emit}$. When the atom column number N in the band becomes larger, the critical K value for dislocation emission, $K_{II}^{\rm emit}$, decreases and eventually approaches an asymptote, see Tan and Yang [56]. This calculation justifies, in some extent, the convergence of the present model to the actual atomistic assembly.

The nonlinear atom motion governed by the above dynamic system controlled by Eq. (46) relies on a loading parameter $\alpha = K_{II}/K_0$, where $K_0 = E'\sqrt{a_0}$. The phase trajectories of the first atom-pair at the crack tip were plotted [56] at various levels of α. It is observed that the phase diagrams become more and more chaotic as α value increases. As a precursor of the dislocation emission from the crack tip, the chaotic atom motion intervenes and dominates the early response near defects. Similar conclusions are reached by other measures on chaotic motion. For examples, strange attractor appears in the Poincarè section diagram of the same dynamic system, and the Lyapunov index takes a pattern shown in Fig. 7.

In Fig. 7, the largest Lyapunov exponent of Eq. (46) is calculated for the load parameters $\alpha = K_{II}/K_0$ varying from 0 to 0.09, when N is taken as 2. The Lyapunov exponent analysis on the equation system (46) reveals its chaotic characteristics. As the load parameter α increases, the crack tip atoms exhibit distinct dynamic responses in the two regimes of α values. For an α value in regime I, atoms vibrate individually near the balanced positions and their motions are almost harmonic. In regime II, nonlinear effect dominates and atoms couple together to approach a state to nucleate dislocations. The regions I and II are separated at an α value of 0.066, at which the maximum Lyapunov exponent rises suddenly. That α value for chaotic atom motion is less than one half of the α value for the static fracture toughness ($\alpha = 0.139$) [56], corresponding to $K_{II}^{\rm emit}$ in Fig. 7. Consequently, the crack tip chaotic atom motion is a precursor of dislocation nucleation.

The result in Fig. 7 suggests that the dynamic dislocation emission process is more intricate than the static one. From the figure we obtain one additional parameter for the dynamic dislocation emission process, namely the $K_{II}^{\rm chaos}$ value at the transition from regime I to regime II. $K_{II}^{\rm chaos}$ refers to the burst of chaos in a dynamic process. Before reaching the value of $K_{II}^{\rm chaos}$, the crack tip remains stationary and is absolutely stable against the dislocation emission. When $K_{II} > K_{II}^{\rm chaos}$, chaotic atom motion occurs prior to dislocation nucleation.

The chaotic nature of dislocation emission is shown by the oscillation of dislocation center along the atom strip. At an intermediate level of K_{II}, dislocations nucleated at the crack tip will drift in the dislocation emission band instead of staying at a fixed location. We call this dynamic phenomenon as *dislocation cloud*. Because of the fast drifting of dislocation core, one can hardly give a deterministic description on the dislocation location. A probabilistic description will be attempted instead. We denote Prob(x_1) as the probability density for a dislocation to be detected at the position x_1. In the process of integrating Eqs.

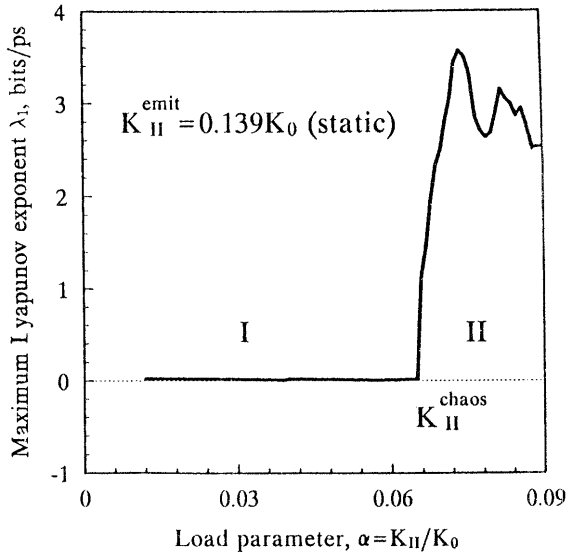

Fig. 7. The maximum Lyapunov exponent λ_1 versus the load parameter α. The curve reveals sudden appearance of chaos in the crack tip atom motion when the applied load exceeds the critical value K_{II}^{chaos}

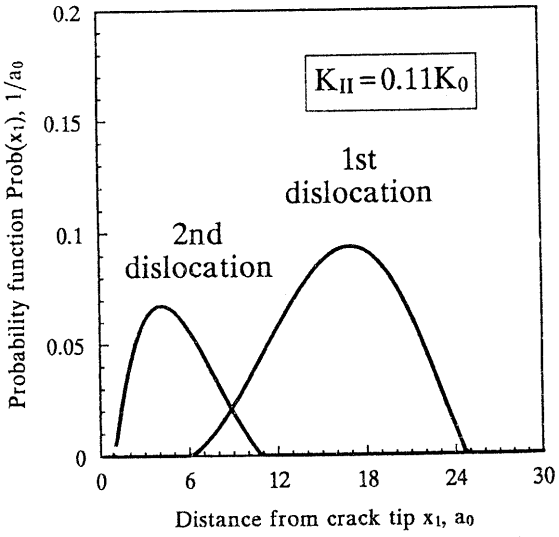

Fig. 8. Curves show the probability functions of the core positions for the first and the second dislocations emitted from the crack tip.

(46), the dislocation positions at every ten integration steps are recorded. Taking the total recording number as n_0 , we define the probability as

$$\text{Prob}(x_1) = \lim_{\Delta x_1 \to 0} \frac{n(x_1; \Delta x_1)}{n_0 \Delta x_1}, \qquad (48)$$

where $n(x_1, \Delta x_1)$ is the recordings of dislocation cores located in the region $[x_1 - \frac{\Delta x_1}{2}, x_1 + \frac{\Delta x_1}{2}]$. Our calculations showed that after the time evolution for about 50ps the curve $\text{Prob}(x_1)$ approaches a steady configuration. What we observe in the conventional microscopic measurement is the time average of the dislocation cloud. The dislocation cloud model predicts an extended core region along the dislocation glide plane, where the recorded data of microscopic deformation are actually the time average of the oscillating dislocation core. Indeed the recent nanomechanics experiment revealed an extended core-region in which the continuum elasticity field is severely perturbed.

Figure 8 shows the probability functions $\text{Prob}_1(x_1)$ and $\text{Prob}_2(x_1)$ for the occurrence of two dislocations that nucleate from a crack tip and drift ahead of it, at a remote loading of $\alpha = 0.11$. The functions $\text{Prob}_1(x_1)$ for the first dislocation and $\text{Prob}_2(x_1)$ for the second one are normalized such that for the first dislocation has a total probability of one, namely $\int_0^\infty \text{Prob}_1(x_1)dx_1 = 1$. There is a segment along x_1 axis ahead of the crack tip where the two probability functions overlap. Both dislocations may enter the overlapping zone, either at different times or at different locations. Under a macroscopically observed time scale, the overlapping dislocation clouds would manifest themselves as connected cores. Ratio of the covered areas by two probability functions shows the occurring rate of the two dislocations. Since $\int_0^\infty \text{Prob}_1(x_1)dx_1 > \int_0^\infty \text{Prob}_2(x_1)dx_1$, the first nucleated dislocation would occasionally drift back to the crack tip and deplete the second dislocation.

The description of the inter-atomic potential certainly influences the possible chaotic motion at the crack tip. Depending on the nature of the inter-atomic potential, dislocations can emit from the crack tip like a passage of solitone or a passage of cloud. The brittle versus ductile behavior of materials is decided by the chaotic atom motion near the crack tip. It is the chaotic competition between the emission of dislocation clouds and the chaotic-to-deterministic separation of cleavage that decides the fracture toughness of a material. Related issues, such as the temperature and rate effects on the brittle versus ductile transition, can also be addressed by the chaotic nature of the atom motion near the crack tip.

7 CONCLUDING REMARKS

Chaotic atom motion near a crack tip excited by fracture are studied in a combined atomistic-continuum approach. Numerical simulations are facilitated by a atom-continuum overlapping belt which can convert the mechanical atmosphere formed on the atom assembly. The defects transmission across the atom-continuum interface are easily addressed. This technique put no extra constraint on the atom assembly. Simplified analytical atom-continuum models put focus on nonlinear effects of the crack tip atom motions. They show effects of the macroscopic controlling parameters on the microscopic atom behaviors.

Acknowledgements

The authors acknowledge the joint supports on this research project by the National Natural Science Foundation of China, and by the State Education Commission of China.

REFERENCES

1. M. Sakai, J. Mater. Res., **8** (1993) 668.
2. M. S. Daw and M. I. Baskes, Phys. Rev. Lett., **50** (1983) 1285.
3. M. S. Daw and M. I. Baskes, Phys. Rev. B, **29** (1984) 6443.
4. M. I. Baskes, J. S. Nelson, and A. F. Wright, Phys. Rev. B, **40** (1989) 6085.
5. M. I. Baskes, Phys. Rev. B, **46** (1992) 2727.
6. G. P. Cherepanov, Mechanics of brittle fracture, Nauka Press, Moscow (1974).
7. Smithells Metals Reference Book, edited by E. A. Brandes (Butterworths, London, 1983).
8. B. deCelis, A. S. Argon, and S. Yip, J. Appl. Phys., **54** (1983) 4864.
9. R. G. Hoagland, M. S. Daw, and J. P. Hirth, J. Mater. Res., **6** (1991) 2565.
10. N. Sasaki, T. Iwasaki, N. Chiba, Y. Abe and Y. Ishikawa, JSME Inter. J., **36** (1990) 50.
11. H. Tan and W. Yang, Acta Mechanica Sinica, **10** (1994) 150.
12. K. S. Cheung, and S. Yip, Model. Simul. Mater. Sci. Eng., **2** (1994) 865.
13. H. Kitagawa, A. Nakatani and Y. Shibutani, Mater. Sci. Eng. A, **176** (1994) 263.
14. T. Iwasaki N. Sasaki, N. Chiba and Y. Abe, JSME Inter. J. A, **37** (1994) 143.
15. H. Kitagawa, and A. Nakatani, JSME Inter. J. A, **38** (1995) 1.
16. M. Mullins and M. A. Dokainish, Phil. Mag. A, **46** (1982) 771.
17. S. Kohlhoff, P. Gumbsch and H. F. Fischmeister, Phil. Mag. A, **64** (1991) 851.
18. W. Yang, H. Tan, and T. F. Guo, Model. Simul. Mater. Sci. Eng., **2** (1994) 767.
19. H. Tan and W. Yang, Acta Mechanica Sinica, **10** (1994) 237.
20. E. Kröner, Int. J. Engng. Sci., **1** (1963) 261.
21. E. Kröner, Int. J. Solids Struct., **3** (1967) 731.
22. H. Tan and W. Yang, Nonlinear motion of atoms at a crack tip during cleavage processes, to appear in Int. J. Fracture, (1995).
23. H. Tan and W. Yang, Catastrophic fracture induced fracto-emission, submitted to J. Mater. Sci., (1995).
24. J. T. Dickinson, S. C. Langford, and L. C. Jensen, J. Mater. Res., **8** (1993) 2921.
25. C. Hsieh and R. Thomson, J. Appl. Phys., 44 (1973) 2051.
26. R. Thomson, V. K. Tewary and K. Masuda-Jindo, J. Mater. Res., **2** (1987) 619.
27. K. Masuda-Jindo, V. K. Tewary and R. Thomson, Mater. Sci. Eng. A, **146** (1991) 273.
28. K. Masuda-Jindo, S. J. Zhou, R. Thomson and A. E. Carlsson, Mater. Sci. Eng. A, **176** (1994) 255.
29. J. E. Sinclair, Phil. Mag., **31** (1975) 647.
30. A. J. Markworth and J. P. Hirth, J. Mater. Sci., **16** (1981) 3405.
31. J. T. Dickinson, E. E. Donaldson and M. K. Park, J. Mat. Sci., **16** (1981) 2897.
32. Y. Enomoto and M. M. Chaudhri, J. Amer. Ceram. Soc., **76** (1993) 2583.
33. J. Fuhrmann, L. Nick, J. T. Dickinson and L. C. Jensen, J. Appl. Polym. Sci., **48** (1993) 2123
34. J. T. Dickinson, L. C. Jensen, S. C. Langford and R. P. Dion, J. Polym. Sci. B, **32** (1994) 993.
35. J. T. Dickinson, L. C. Jensen, S. C. Langford and R. G. Hoagland, J. Mater. Res., **9** (1994) 1156.
36. S. C. Langford, Z. Ma and J. T. Dickinson, J. Mater. Res., 4 (1989) 1272.
37. D. W. Short, R. A. Rapp and J. P. Hirth, J. Chem. Phys., **57** (1972) 1381.
38. K. A. Zimmerman, S. C. Langford, J. T. Dickinson and R. P. Dion, J. Polym. Sci., **31** (1993) 1229.
39. M. P. Tosi, in Solid State Physics, vol. 16, edited by F. Seitz and D. Turnbull (New York, Academic, 1964) 1.
40. J.J. Gilman, Fracture (John Wiley, New York, 1959).
41. C. S. Barrett and T. B. Massalski, Structure of Metals (McGraw-Hills, New York, 1966).
42. Y. L. Tsai and J. J. Mecholsky, J. Mater. Res., **6** (1991) 1248.
43. J. J. Mecholsky and T. J. Mackin, J. Mater. Sci. Lett., **7** (1988) 1145.
44. J. J. Mecholsky, T. J. Mackin and D. E. Passoja, Adv. Ceram., **22** (1988) 127.
45. J. J. Mecholsky, D. E. Passoja and K. S. Feinberg, J. Am. Ceram. Soc., **72** (1989) 60.
46. J. T. Dickinson, L. C. Jensen, S. C. Langford and J. P. Hirth, J. Mater. Res., **6** (1991) 112.
47. M. L. A. Nip, J. A. Tuszynski, Z. W. Gortel and T. A. Riauka, Physical Review, **B48** (1993) 15732.
48. A. J. Markworth, Materials Letters, **2** (1984) 333.
49. A. J. Markworth, Journal of Materials Science Letters, **3** (1984) 210.
50. A. J. Markworth, K. J. McCoy and R. W. Rollins, Journal of Materials Res., **3** (1988) 675.
51. R. Mohan, A. J. Markworth and R. W. Rollins, Model. Simul. Mater. Sci. Eng., **2** (1994) 659.
52. J. S. Wolf, H. L. Swinney, J. A. Vastano, Physica D, **16** (1985) 285.
53. J. R. Rice, J. Mech. Phys. Solids, **40** (1992) 239.
54. Y. Sun, G. E. Beltz and J. R. Rice, Mater. Sci. Eng., **A170** [1993] 67.
55. M. Doyama, Mater. Sci. Eng. A, **176** (1994) 277.
56. H. Tan and W. Yang, Nonlinear motion of crack tip atoms during dislocation emission processes, to appear in J. Appl. Phys., Dec. 15 (1995).
57. L. B. Freund, Dynamic Fracture Mechanics, Cambridge Press (1990), 112.